INTERNATIONAL JOURNAL FOR NUMERICAL METHODS IN FLUIDS
Int. J. Numer. Meth. Fluids 2002; **38**:881–893 (DOI: 10.1002/fld.248)

On the use of the Galerkin method for 3D numerical modelling of the general circulation: the South Atlantic experiment

Joseph Harari*,† and Emanuel Giarolla‡

Instituto Oceanográfico da USP, Praça do Oceanográfico, 191, 05508-900—São Paulo—SP, Brazil

SUMMARY

A linear three-dimensional hydrodynamical numerical model, with the application of the Galerkin Method for the vertical dependence, is here presented. The spherical coordinate system is used, in order to allow large-scale simulations. The equations and mathematical development of the model are shown in detail, together with the boundary and initial conditions, and the sequence of equations' solution. The model is applied to the South Atlantic Ocean, for estimating typical seasonal circulations, and the results are summarized in maps of currents at surface and 1000 m depth, and in transport values of the Brazil Current between 30°S and 40°S. Copyright © 2002 John Wiley & Sons, Ltd.

KEY WORDS: ocean general circulation model; Galerkin method; spectral method

1. INTRODUCTION

In the last few years, several ocean general circulation models (OGCM) were implemented in the study of oceanic dynamical processes. This may be atributted to the continuous improvement of observations and computational resources, which allow the use of more realistic bathymetry, better parametrizations, finer grid resolutions, corrected surface wind values, etc.

Since the pioneer works of Sarkisyan (in: Bryan [1]) and Bryan [1], several large-scale ocean numerical models were proposed; at present, four types of models are used, with differences in the vertical solution of the basic equations: models with linear vertical z coordinate, with either constant or variable vertical grid spacing (e.g. Reference [2]); models with sigma vertical coordinates, which are normalized according to topography (e.g. the Princeton Ocean Model POM; Reference [3]); isopycnal layer models, where the ocean is reduced to a pack of layers, each one with constant potential density values (e.g. the Miami Isopycnic Coordinate

* Correspondence to: J. Harari, Instituto Oceanografico da USP, Praca do Oceanografico 191, 05508-900—Sao Paulo—SP, Brazil.
† E-mail: joharari@usp.br
‡ E-mail: emanuėl@cptec.inpe.br

Received 2 May 1997
Revised 25 July 2001

Ocean Model MICOM; Reference [4]); and spectral models, where the unknown variables are represented through expansions with given basis functions for the vertical dependence (e.g. Reference [5]).

The model presented here uses the spectral solution together with the Galerkin method. The dependent variables (velocity components u and v, density, etc.) are represented by expansions as products of 2D coefficients (which account for the horizontal and time dependence) and basis functions (for the vertical variations). These expansions are inserted into the hydrodynamic equations, which are then multiplied by the respective basis functions and vertically integrated, from the surface to the bottom. The final model equations allow the computations of the horizontal variations and time evolutions of the 2D coefficients and the recovering of the 3D fields through the initial expansions.

Davies [5, 6] presented the formulation of a three-dimensional wind-induced model using the spectral method and compared the results of this formulation against the direct finite difference solution in the vertical (Reference [7]); applications of the spectral methodology in stratified seas are given in Davies [8].

At present, however, only few publications related to large-scale ocean circulation are based on the spectral solution, perhaps due to the complexity of its formulation or the heavy computational effort that is necessary when the number of degrees of freedom (modes) is large. On the other hand, this solution has two important advantages: considering that the equations are vertically integrated, the three-dimensional problem is reduced to a set of two-dimensional ones; besides, the dependent variables may be computed at any level of interest (although with an accuracy that depends on the choice of suitable basis functions, among other factors).

The objective of this work is to present a general circulation ocean model of the South Atlantic Ocean based on the spectral solution. This first version of the model considers only the linear terms of the basic hydrodynamical equations and the density field is made time-invariant. The model is forced by seasonal winds (constant in time). Note that the spectral solution may also be used in full non-linear thermodynamic problems, with variable winds and radiational effects, but that requires more computational resources and shall be presented in future researches.

In the next sections the model mathematical development will be presented, followed by some numerical experiments and a discussion about the obtained results.

2. THE MODEL DESCRIPTION

This model is based on Davies [6] formulation, using spherical coordinates, for large-scale oceanic simulations. In this first version of the model, the non-linear terms were neglected, which greatly simplifies the mathematical formulation. Although the linearization removes important effects such as meso-scale eddies associated with strong currents, it allows the investigation of the linear response of the ocean to the atmospheric forcings, pointing out the contribution of linear effects in the oceanic processes.

Another simplification of this model is the assumption of a time-invariant density field, eliminating thus the equations for temperature, salinity and density—and restricting the number of unknowns to three: the two horizontal velocity components and the vertical displacements of the density surfaces. This simplification considerably reduces the computational time to reach the model spin-up, since only mechanical forces are considered (the wind stresses),

being suitable when the interest is restricted to the wind-driven currents and does not include the thermohaline circulation.

Note that the spectral solution may also be used in full non-linear thermodynamic problems, with variable winds and radiational effects, but that requires more computational resources and shall be presented in future researches.

2.1. Model formulation

The model is composed of the prognostic equations

$$\frac{\partial u}{\partial t} - 2\Omega \sin\varphi v = \frac{-1}{\bar{\rho} R \cos\varphi} \frac{\partial p}{\partial \lambda} + \frac{\partial}{\partial z}\left(N \frac{\partial u}{\partial z}\right) + T_u \tag{1}$$

$$\frac{\partial v}{\partial t} + 2\Omega \sin\varphi u = \frac{-1}{\bar{\rho} R} \frac{\partial p}{\partial \varphi} + \frac{\partial}{\partial z}\left(N \frac{\partial v}{\partial z}\right) + T_v \tag{2}$$

and the diagnostic equations

$$\frac{1}{R\cos\varphi}\left(\frac{\partial u}{\partial \lambda} + \frac{\partial (v\cos\varphi)}{\partial \varphi}\right) + \frac{\partial w}{\partial z} = 0 \tag{3}$$

$$\frac{\partial p}{\partial z} = \rho g \tag{4}$$

where u, v and w are the current components (to east, north and downward, respectively), λ and φ are respectively, longitude and latitude (positive to east and north), z is the depth (positive downward), t is the time, R is the Earth radius, Ω is the angular velocity of the Earth rotation, g is the gravity acceleration, ρ is the sea water density, $\bar{\rho}$ is the mean sea water density, p is the pressure, N is the coefficient of vertical eddy viscosity and N_h is the coefficient of horizontal eddy viscosity. T_u and T_v are the horizontal turbulent diffusivity terms, defined by

$$T_u = N_\mathrm{h} \nabla_h^2 u + \frac{N_\mathrm{h}}{R^2}\left[\left(1 - \frac{\sin^2\varphi}{\cos^2\varphi}\right)u - \frac{2\sin\varphi}{\cos^2\varphi}\frac{\partial v}{\partial \lambda}\right] \tag{5}$$

$$T_v = N_\mathrm{h} \nabla_h^2 v + \frac{N_\mathrm{h}}{R^2}\left[\left(1 - \frac{\sin^2\varphi}{\cos^2\varphi}\right)v - \frac{2\sin\varphi}{\cos^2\varphi}\frac{\partial u}{\partial \lambda}\right] \tag{6}$$

Representing the vertical velocity w as the displacement of a density surface η, w can be written as

$$w = -\frac{\partial \eta}{\partial t} \tag{7}$$

Integrating the hydrostatic relationship (4) from the surface to the bottom, results in

$$p = p_a + \rho_0 g \eta_0 + g \int_0^z \rho \, \mathrm{d}z' \tag{8}$$

where p_a is the atmospheric pressure, ρ_0 and η_0 are the density at the sea surface and the sea surface height, respectively. Inserting the expressions of $T_u, T_v w$ and p ((7)–(8)) into the basic equations (1)–(4), the model equations become

$$\frac{\partial u}{\partial t} - 2\Omega \sin\varphi v = \frac{-1}{\bar{\rho} R \cos\varphi}\frac{\partial p_a}{\partial \lambda} - \frac{g\rho_0}{\bar{\rho} R\cos\varphi}\frac{\partial \eta_0}{\partial \lambda} - \frac{g}{\bar{\rho} R\cos\varphi}\frac{\partial}{\partial \lambda}\left[\int_0^z \rho\, dz'\right] + \frac{\partial}{\partial z}\left[N\frac{\partial u}{\partial z}\right] + \frac{N_h}{R^2\cos^2\varphi}\frac{\partial^2 u}{\partial \lambda^2} - \frac{N_h \sin\varphi}{R^2\cos\varphi}\frac{\partial u}{\partial \varphi} + \frac{N_h}{R^2}\frac{\partial^2 u}{\partial \varphi^2} + \frac{N_h}{R^2}\left(1 - \frac{\sin^2\varphi}{\cos^2\varphi}\right)u - \frac{2N_h}{R^2}\frac{\sin\varphi}{\cos^2\varphi}\frac{\partial v}{\partial \lambda} \tag{9}$$

$$\frac{\partial v}{\partial t} + 2\Omega \sin\varphi u = \frac{-1}{\bar{\rho} R}\frac{\partial p_a}{\partial \varphi} - \frac{g\rho_0}{\bar{\rho} R}\frac{\partial \eta_0}{\partial \varphi} - \frac{g}{\bar{\rho} R}\frac{\partial}{\partial \varphi}\left[\int_0^z \rho\, dz'\right] + \frac{\partial}{\partial z}\left[N\frac{\partial v}{\partial z}\right] + \frac{N_h}{R^2\cos^2\varphi}\frac{\partial^2 v}{\partial \lambda^2} - \frac{N_h \sin\varphi}{R^2\cos\varphi}\frac{\partial v}{\partial \varphi} + \frac{N_h}{R^2}\frac{\partial^2 v}{\partial \varphi^2} + \frac{N_h}{R^2}\left(1 - \frac{\sin^2\varphi}{\cos^2\varphi}\right)v + \frac{2N_h}{R^2}\frac{\sin\varphi}{\cos^2\varphi}\frac{\partial u}{\partial \lambda} \tag{10}$$

and

$$\frac{\partial}{\partial t}\left(\frac{\partial \eta}{\partial z}\right) - \frac{1}{R\cos\varphi}\left(\frac{\partial u}{\partial \lambda} + \frac{\partial (v\cos\varphi)}{\partial \varphi}\right) = 0 \tag{11}$$

Expressions (9)–(11) are thus the basic model's equations, for the unknowns u, v and η.

The model equations are subject to boundary conditions at the surface ($z = 0$), corresponding to the wind stress $\boldsymbol{\tau}_s$, with wind components F_0 and G_0 related to the wind velocity W and its components W_λ and W_φ:

$$F_0 = c_D \rho_a W W_\lambda \tag{12}$$

$$G_0 = c_D \rho_a W W_\varphi \tag{13}$$

where ρ_a is the air density and c_D is the drag coefficient. The values adopted for ρ_a and c_D were extracted from Hellerman [9].

The bottom boundary conditions (at $z = h$) correspond to the linear relation between the bottom stress and current components

$$F_B = k\rho u \tag{14}$$

$$G_B = k\rho v \tag{15}$$

where k is the bottom drag coefficient; additionally, at the bottom

$$\eta = 0 \quad \text{at } z = h \tag{16}$$

$$\frac{\mathrm{d}(z-h)}{\mathrm{d}t} = 0 \quad \text{at } z = h \tag{17}$$

The spectral solution (in conjunction with the Galerkin method) involves the expansion of the dependent variables u, v and η in terms of products of 2D coefficients and basis functions and the insertion of these expansions into the basic equations. Afterwards, the resulting equations are multiplied by the respective basis functions and vertically integrated. In order to avoid different vertical integrations at each grid point (due to different values of the depths h), the vertical interval $(0,h)$ is replaced by the constant interval (a,b), through a sigma coordinate transform:

$$\xi = (b-a)\frac{z}{h} + a \tag{18}$$

Using the above expression, the partial derivatives involving the spatial coordinates become

$$\frac{\partial}{\partial\lambda} \equiv \left(\frac{\partial}{\partial\lambda} - \frac{\xi-a}{h}\frac{\partial h}{\partial\lambda}\frac{\partial}{\partial\xi}\right) \tag{19}$$

$$\frac{\partial}{\partial\varphi} \equiv \left(\frac{\partial}{\partial\varphi} - \frac{\xi-a}{h}\frac{\partial h}{\partial\varphi}\frac{\partial}{\partial\xi}\right) \tag{20}$$

$$\frac{\partial}{\partial z} \equiv \left(\frac{b-a}{h}\frac{\partial}{\partial\xi}\right) \tag{21}$$

from which expressions can be obtained for $\partial^2/\partial\lambda^2$ and $\partial^2/\partial\varphi^2$.

The dependent variables u, v and η are then expanded in terms of coefficients A_r, B_r and C_r (which account for the horizontal and time variations) and basis functions f and ψ (for the vertical variations), as follows:

$$u(\lambda,\varphi,\xi,t) = \sum_{r=1}^{M} A_r(\lambda,\varphi,t) f_r(\xi) \tag{22}$$

$$v(\lambda,\varphi,\xi,t) = \sum_{r=1}^{M} B_r(\lambda,\varphi,t) f_r(\xi) \tag{23}$$

$$\eta(\lambda,\varphi,\xi,t) = \sum_{r=1}^{M} C_r(\lambda,\varphi,t) \psi_r(\xi) \tag{24}$$

where M is the number of terms used in the expansions.

According to Davies [6], the density field ρ and the coefficient of vertical eddy viscosity N can also be expanded similarly, in terms of 2D coefficients D_r and E_r and basis functions ϕ and ξ:

$$\rho(\lambda,\varphi,\xi,t) = \sum_{r=1}^{M} D_r(\lambda,\varphi,t) \phi_r(\xi) \tag{25}$$

$$N(\lambda,\varphi,\xi,t)=\sum_{r=1}^{M'}E_r(\lambda,\varphi,t)\chi_r(\xi) \tag{26}$$

where M' is the number of terms used in the expansion of N, which can be equal or not equal to M.

In the above expansions, f, ψ, ϕ and ξ are functions chosen beforehand so that D_r and E_r are determined by the adopted values of ρ and N, respectively.

The final form of the continuity equation (11) is obtained after inserting the expansions, multiplying by the basis function (ψ) and integrating in the vertical (from a to b), so that

$$\begin{aligned}
&\sum_{s=1}^{M}\frac{\partial C_s}{\partial t}\int_a^b\frac{\partial\psi_s}{\partial\xi}\psi_r\,\mathrm{d}\xi\\
&\quad-\frac{h}{b-a}\frac{1}{R\cos\varphi}\left\{\sum_{s=1}^{M}\left[\left(\frac{\partial A_s}{\partial\lambda}+\cos\varphi\frac{\partial B_s}{\partial\varphi}-B_s\sin\varphi\right)\int_a^b f_s\psi_r\,\mathrm{d}\xi\right]\right\}\\
&\quad+\frac{1}{b-a}\frac{1}{R\cos\varphi}\left\{\sum_{s=1}^{M}\left[\left(A_s\frac{\partial h}{\partial\lambda}+B_s\cos\varphi\frac{\partial h}{\partial\varphi}\right)\int_a^b(\xi-a)\frac{\partial f_s}{\partial\xi}\psi_r\,\mathrm{d}\xi\right]\right\}=0\\
&\quad r=1,2,\ldots,M
\end{aligned} \tag{27}$$

The same procedure is applied to the equations for the horizontal components of the velocity ((9)–(10)), resulting in the equations for A_r and B_r

$$\begin{aligned}
&\sum_{s=1}^{M}\frac{\partial A_s}{\partial t}\int_a^b f_sf_r\,\mathrm{d}\xi-2\Omega\sin\varphi\sum_{s=1}^{M}B_s\int_a^b f_sf_r\,\mathrm{d}\xi\\
&=-\frac{1}{\bar\rho R\cos\varphi}\frac{\partial p_a}{\partial\lambda}\int_a^b f_r\,\mathrm{d}\xi-\frac{g\rho(a)}{\bar\rho R\cos\varphi}\frac{\partial\eta_0}{\partial\lambda}\int_a^b f_r\,\mathrm{d}\xi\\
&\quad-\frac{g}{\bar\rho R\cos\varphi}\frac{1}{b-a}\sum_{s=1}^{M}\left\{\frac{\partial}{\partial\lambda}(D_sh)\int_a^b\int_a^{\xi}\phi_s\,\mathrm{d}\xi' f_r\,\mathrm{d}\xi\right\}\\
&\quad+\frac{g}{\bar\rho R\cos\varphi}\frac{\partial h}{\partial\lambda}\frac{1}{b-a}\sum_{s=1}^{M}D_s\int_a^b(\xi-a)\phi_sf_r\,\mathrm{d}\xi\\
&\quad+\frac{F_0}{\rho(a)}\frac{b-a}{h}f_r(a)-\frac{F_B}{\rho(b)}\frac{b-a}{h}f_r(b)\\
&\quad-\frac{(b-a)^2}{h^2}\sum_{s=1}^{M}\sum_{l=1}^{M'}A_sE_l\int_a^b\chi_l\frac{\partial f_s}{\partial\xi}\frac{\partial f_r}{\partial\xi}\,\mathrm{d}\xi+\frac{N_{\mathrm{h}}}{R^2\cos^2\varphi}\sum_{s=1}^{M}\left\{\frac{\partial^2A_s}{\partial\lambda^2}\int_a^b f_sf_r\,\mathrm{d}\xi\right.\\
&\quad\left.+\left[\frac{2A_s}{h^2}\left(\frac{\partial h}{\partial\lambda}\right)^2-\frac{2}{h}\frac{\partial h}{\partial\lambda}\frac{\partial A_s}{\partial\lambda}-\frac{A_s}{h}\frac{\partial^2h}{\partial\lambda^2}\right]\int_a^b(\xi-a)\frac{\partial f_s}{\partial\xi}f_r\,\mathrm{d}\xi\right.
\end{aligned}$$

$$+\frac{A_s}{h^2}\left(\frac{\partial h}{\partial \lambda}\right)^2\int_a^b(\xi-a)^2\,\frac{\partial^2 f_s}{\partial \xi^2}\,f_r\,\mathrm{d}\xi\Bigg\}-\frac{N_\mathrm{h}\sin\varphi}{R^2\cos\varphi}\sum_{s=1}^{M}\Bigg\{\frac{\partial A_s}{\partial\varphi}\int_a^b f_s f_r\,\mathrm{d}\xi$$

$$-\frac{A_s}{h}\,\frac{\partial h}{\partial\varphi}\int_a^b(\xi-a)\,\frac{\partial f_s}{\partial\xi}\,f_r\,\mathrm{d}\xi\Bigg\}+\frac{N_\mathrm{h}}{R^2}\sum_{s=1}^{M}\Bigg\{\frac{\partial^2 A_s}{\partial\varphi^2}\int_a^b f_s f_r\,\mathrm{d}\xi$$

$$+\left[\frac{2A_s}{h^2}\left(\frac{\partial h}{\partial\varphi}\right)^2-\frac{2}{h}\,\frac{\partial h}{\partial\varphi}\,\frac{\partial A_s}{\partial\varphi}-\frac{A_s}{h}\,\frac{\partial^2 h}{\partial\varphi^2}\right]\int_a^b(\xi-a)\,\frac{\partial f_s}{\partial\xi}\,f_r\,\mathrm{d}\xi$$

$$+\frac{A_s}{h^2}\left(\frac{\partial h}{\partial\varphi}\right)^2\int_a^b(\xi-a)^2\,\frac{\partial^2 f_s}{\partial\xi^2}\,f_r\,\mathrm{d}\xi\Bigg\}+\frac{N_\mathrm{h}}{R^2}\left(1-\frac{\sin^2\varphi}{\cos^2\varphi}\right)\sum_{s=1}^{M}A_s\int_a^b f_s f_r\,\mathrm{d}\xi$$

$$-\frac{2N_\mathrm{h}}{R^2}\,\frac{\sin\varphi}{\cos^2\varphi}\sum_{s=1}^{M}\Bigg\{\frac{\partial B_s}{\partial\lambda}\int_a^b f_s f_r\,\mathrm{d}\xi-\frac{B_s}{h}\,\frac{\partial h}{\partial\lambda}\int_a^b(\xi-a)\,\frac{\partial f_s}{\partial\xi}\,f_r\,\mathrm{d}\xi\Bigg\}$$

$$r=1,2,\ldots,M \tag{28}$$

$$\sum_{s=1}^{M}\frac{\partial B_s}{\partial t}\int_a^b f_s f_r\,\mathrm{d}\xi+2\Omega\sin\varphi\sum_{s=1}^{M}A_s\int_a^b f_s f_r\,\mathrm{d}\xi$$

$$=-\frac{1}{\bar\rho R}\,\frac{\partial p_a}{\partial\varphi}\int_a^b f_r\,\mathrm{d}\xi-\frac{g\rho(a)}{\bar\rho R}\,\frac{\partial\eta_0}{\partial\varphi}\int_a^b f_r\,\mathrm{d}\xi$$

$$-\frac{g}{\bar\rho R}\,\frac{1}{b-a}\sum_{s=1}^{M}\Bigg\{\frac{\partial}{\partial\varphi}(D_s h)\int_a^b\int_a^{\xi}\phi_s\,\mathrm{d}\xi' f_r\,\mathrm{d}\xi\Bigg\}$$

$$+\frac{g}{\bar\rho R}\,\frac{\partial h}{\partial\varphi}\,\frac{1}{b-a}\sum_{s=1}^{M}D_s\int_a^b(\xi-a)\phi_s f_r\,\mathrm{d}\xi$$

$$+\frac{G_0}{\rho(a)}\,\frac{b-a}{h}\,f_r(a)-\frac{G_B}{\rho(b)}\,\frac{b-a}{h}\,f_r(b)-\frac{(b-a)^2}{h^2}\sum_{s=1}^{M}\sum_{l=1}^{M'}B_s E_l\int_a^b\chi_l\,\frac{\partial f_s}{\partial\xi}\,\frac{\partial f_r}{\partial\xi}\,\mathrm{d}\xi$$

$$+\frac{N_\mathrm{h}}{R^2\cos^2\varphi}\sum_{s=1}^{M}\Bigg\{\frac{\partial^2 B_s}{\partial\lambda^2}\int_a^b f_s f_r\,\mathrm{d}\xi+\left[\frac{2B_s}{h^2}\left(\frac{\partial h}{\partial\lambda}\right)^2-\frac{2}{h}\,\frac{\partial h}{\partial\lambda}\,\frac{\partial B_s}{\partial\lambda}-\frac{B_s}{h}\,\frac{\partial^2 h}{\partial\lambda^2}\right]$$

$$\times\int_a^b(\xi-a)\,\frac{\partial f_s}{\partial\xi}\,f_r\,\mathrm{d}\xi+\frac{B_s}{h^2}\left(\frac{\partial h}{\partial\lambda}\right)^2\int_a^b(\xi-a)^2\,\frac{\partial^2 f_s}{\partial\xi^2}\,f_r\,\mathrm{d}\xi\Bigg\}$$

$$-\frac{N_\mathrm{h}\sin\varphi}{R^2\cos\varphi}\sum_{s=1}^{M}\Bigg\{\frac{\partial B_s}{\partial\varphi}\int_a^b f_s f_r\,\mathrm{d}\xi-\frac{B_s}{h}\,\frac{\partial h}{\partial\varphi}\int_a^b(\xi-a)\,\frac{\partial f_s}{\partial\xi}\,f_r\,\mathrm{d}\xi\Bigg\}$$

$$+\frac{N_\mathrm{h}}{R^2}\sum_{s=1}^{M}\Bigg\{\frac{\partial^2 B_s}{\partial\varphi^2}\int_a^b f_s f_r\,\mathrm{d}\xi+\left[\frac{2B_s}{h^2}\left(\frac{\partial h}{\partial\varphi}\right)^2-\frac{2}{h}\,\frac{\partial h}{\partial\varphi}\,\frac{\partial B_s}{\partial\varphi}-\frac{B_s}{h}\,\frac{\partial^2 h}{\partial\varphi^2}\right]$$

$$\times \int_a^b (\xi - a) \frac{\partial f_s}{\partial \xi} f_r \, \mathrm{d}\xi + \frac{B_s}{h^2} \left(\frac{\partial h}{\partial \varphi} \right)^2 \int_a^b (\xi - a)^2 \frac{\partial^2 f_s}{\partial \xi^2} f_r \, \mathrm{d}\xi \Bigg\}$$

$$+ \frac{N_\mathrm{h}}{R^2} \left(1 - \frac{\sin^2 \varphi}{\cos^2 \varphi} \right) \sum_{s=1}^{M} B_s \int_a^b f_s f_r \, \mathrm{d}\xi + \frac{2N_\mathrm{h}}{R^2} \frac{\sin \varphi}{\cos^2 \varphi}$$

$$\times \sum_{s=1}^{M} \left\{ \frac{\partial A_s}{\partial \lambda} \int_a^b f_s f_r \, \mathrm{d}\xi - \frac{A_s}{h} \frac{\partial h}{\partial \lambda} \int_a^b (\xi - a) \frac{\partial f_s}{\partial \xi} f_r \, \mathrm{d}\xi \right\} \quad r = 1, 2, \ldots, M \tag{29}$$

Note that A_r, B_r and C_r become the unknowns of the final model equations (27)–(29).

2.2. Initial conditions

The simulations start from the rest, so

$$A_r = B_r = C_r = 0 \quad \text{at } t = 0 \tag{30}$$

The inclusion of the density field in the model, at $t = 0$, is made through the computation of the values of D_r: the expansion for the density (25) is multiplied by ϕ_s and integrated from a to b, which gives

$$\sum_{r=1}^{M} D_r(\lambda, \varphi, 0) \int_a^b \phi_r(\xi) \phi_s(\xi) \, \mathrm{d}\xi = \int_a^b \rho(\lambda, \varphi, \xi, 0) \, \phi_s(\xi) \, \mathrm{d}\xi \quad s = 1, 2, \ldots, M \tag{31}$$

The above equation, solved in matrix form with a given density field ρ, computes the values of D_r (which were kept constant in the model processing).

With a similar expression, E_r is determined from the given coefficients N:

$$\sum_{r=1}^{M'} E_r \int_a^b \chi_r \chi_s \, \mathrm{d}\xi = \int_a^b N \chi_s \, \mathrm{d}\xi \tag{32}$$

2.3. Boundary conditions

In the model, the sea surface elevation $\eta_0 = \eta(\lambda, \varphi, \xi = a, t)$ is prescribed at all the open boundaries.

The vertical profiles of u and v are also prescribed at the open boundaries, with the correspondent coefficients A_r and B_r computed by solving the following equations in matrix form

$$\sum_{r=1}^{M} A_r \int_a^b f_r f_s \, \mathrm{d}\xi = \int_a^b u f_s \, \mathrm{d}\xi \tag{33}$$

and

$$\sum_{r=1}^{M} B_r \int_a^b f_r f_s \, \mathrm{d}\xi = \int_a^b v f_s \, \mathrm{d}\xi \tag{34}$$

At the closed boundaries, 'no-slip' conditions are used, with $A_r = 0$ at eastern limits and $B_r = 0$ at northern ones.

2.4. The sequence of the equation's solutions

The grid used in this model is Arakawa's 'C' grid, so that equations (27)–(29) are discretized with finite differences forward in time and centred in space. For the time integration, the 'forward–backward' numerical scheme is used.

Initially, the model starts from the rest, so the initial conditions (30) are applied. The values of coefficients D_r and E_r are computed through the given fields of ρ and N, by using relations (31)–(32).

The evolution in time of the model equations is then performed with the following steps:

1. The equation of continuity (27) renews the values of C_r. An 'horizontal filter'

$$C'(i,j) = \alpha C(i,j) + \beta[C(i-1,j) + C(i+1,j) + C(i,j-1) + C(i,j+1)] \tag{35}$$

$$\alpha + 4\beta = 1 \tag{36}$$

   is applied at each time step, in order to avoid numerical instabilities.
2. The model forcings are specified: the wind components and the atmospheric pressure at the sea surface. The values of the sea surface elevations and vertical current profiles at the open boundaries are then prescribed, given the correspondent values of η_0 and coefficients A_r, B_r (through (33) and (34)).
3. The wind stresses are computed with the bulk formulation (12) and (13) and the bottom stress with the linear law (14) and (15).
4. Equation (28) renews the values of A_r.
5. Equation (29) renews the values of B_r.
6. The computed fields of A_r and B_r can be filtered by (35) and (36), but not necessarily at each time step.
7. After the time evolution of coefficients A_r, B_r and C_r, the dependent variables u, v and η can be computed at any depth, by expansions (22)–(24); the sea surface elevation is also computed, as the value of η for $\xi = 0$.

3. MODEL SETTINGS AND EXPERIMENTS

Fourth-order B-Splines functions were used as basis functions f, ψ, ϕ and χ. The B-Splines are polynomious, different from zero only in a finite interval of the domain, centred at points named 'knots'. Davies [6] demonstrated that this basis functions are particularly suitable for internal shear reproduction and have an additional advantage of flexibility for higher resolution in any layer, such as the surface or the pycnocline. The number of terms in the expansions were defined as $M = M' = 6$. The vertical domain $[a,b]$ was set to $[0,1]$, and the knots of the basis functions were equally distributed at $\xi = -1.00,\ -0.66,\ -0.33,\ 0.00,\ 0.33,\ 0.66,\ 1.00,\ 1.33,\ 1.66$ and 2.00.

The vertical profile adopted in this work has the surface layer from surface to the 26.20 potential density surface, the thermocline from surfaces 26.20 to 27.50 and the bottom layer from 27.50 to 29.00 surfaces. The chosen profiles of the coefficient of vertical eddy viscosity had values of $1000\,\mathrm{cm^2\,s^{-1}}$ at the surface layer, $10\,\mathrm{cm^2\,s^{-1}}$ in the thermocline and $100\,\mathrm{cm^2\,s^{-1}}$ at the bottom layer; according to Davies [6], this structure of N represents the realistic high

vertical diffusion at the surface and the minimum vertical transfer of momentum through the pycnocline.

The model was applied to the South Atlantic Basin (5°S–40°S, 60°W–20°E), with a horizontal resolution of $0.5° \times 0.5°$. The ocean topography was extracted from the ETOPO5 database, and a 1000 m cutoff depth was chosen in the experiments, because of the interest only in large-scale circulation. Two experiments were performed, for summer and winter mean conditions. The three-dimensional summer and winter mean densities were prescribed based on values given by Gorshkov [10], and the mean seasonal values of surface winds and atmospheric pressure were extracted from Hellerman [9] and Van Loon [11], respectively. At the open boundaries (northern and southern boundaries of the basin), dynamic height values from Dephant [12] together with altimetric observations from Carton [13] were used to define sea surface height values; and current profiles at the open boundaries were derived from Meehl [14] at the surface and Gorshkov [10] at greater depths.

The other model's parameters were adjusted after preliminary experiments, with values of the bottom drag coefficient $k = 5 \text{ cm s}^{-1}$, the horizontal eddy coefficient $N = 4 \times 10^8 \text{ cm}^2 \text{ s}^{-1}$ and the frequency for spatial filtering of the fields A_r and B_r, corresponding to once in every 30 time steps. The time step adopted was 60 s.

4. MODEL RESULTS

Figure 1 shows the model currents at the surface for the experiment considering mean summer conditions. To obtain this field, the currents values at surface were recovered using the 2D coefficients A_r and B_r in the expansions for u (22) and v (23), considering $\xi = 0$. In this figure, the currents represent the linear response of the ocean to the atmospheric mechanical forcing correspondent to the wind stress. The absence of mesoscale eddies associated with

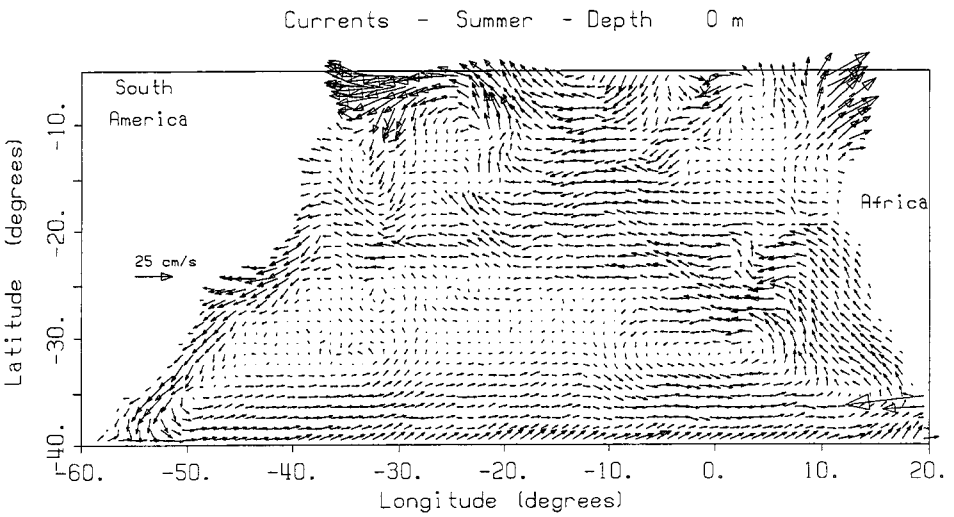

Figure 1. Mean summer horizontal currents at surface.

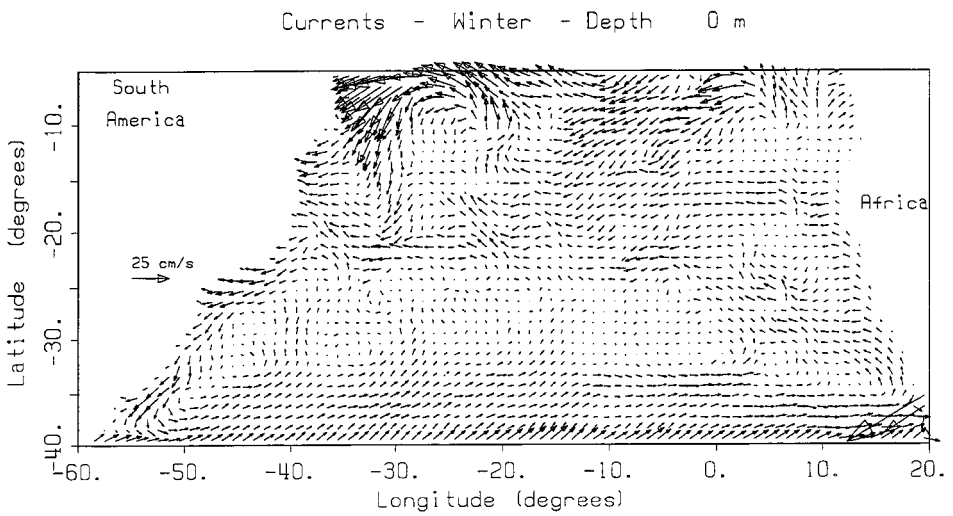

Figure 2. Mean winter horizontal currents at surface.

the currents flow is noticeable, obviously due to their strong non-linear characteristics, which were excluded in this version of the model. The main known dynamic features in the South Atlantic captured by the model are the Brazil Current, flowing southward close to South America, with a recirculation cell, and the Benguela Current, flowing northward close to Africa, within another recirculation cell.

The mean values of Brazil current vary from 8 cm s^{-1} at 30°–31°S to 17 cm s^{-1} at 35°–36°S. The southward transport of the Brazil Current was estimated using values of mean velocity from 0 to 500 m depth, in a zonal section of six offshore grid points (approximately 250 km). Values of 7 Sv were obtained for latitudes between 37.5°S and 38°S (1 Sv = 10^6 m^3 s^{-1}). Garzoli and Bianchi [15] estimated the mean value of 10 Sv in this area, from inverted echo sounders data (November 1984–June 1985), using the 800 m depth as level of reference.

Figure 2 shows the model results for mean winter conditions. In this season, a weakening of the wind systems over the South Atlantic occurs, with a consequent weakening of the currents at the basin scale. The Brazil Current estimated at 30°–31°S is 5.5 cm s^{-1} in this case, and increases to 8 cm s^{-1} at 35°–36°S. The transport estimated at 37.5°–38°S is 5.5 Sv, a half of the 11 Sv value obtained by Garzoli and Garrafo [16] from inverted echo sounders from June 1985 to March 1986.

The currents at 1000m depth were also recovered from the expansions for u and v, using the calculated values for A_r and B_r, and the level ξ equivalent to 1000 m depth (Equation (18)). The Brazil Current and Benguela Current are present at the 1000 m depth level, both in summer and winter results (Figures 3 and 4), although with much less intensities than at the surface. The Brazil Current, in summer and winter, has values of about 8 cm s^{-1} in almost all its extension.

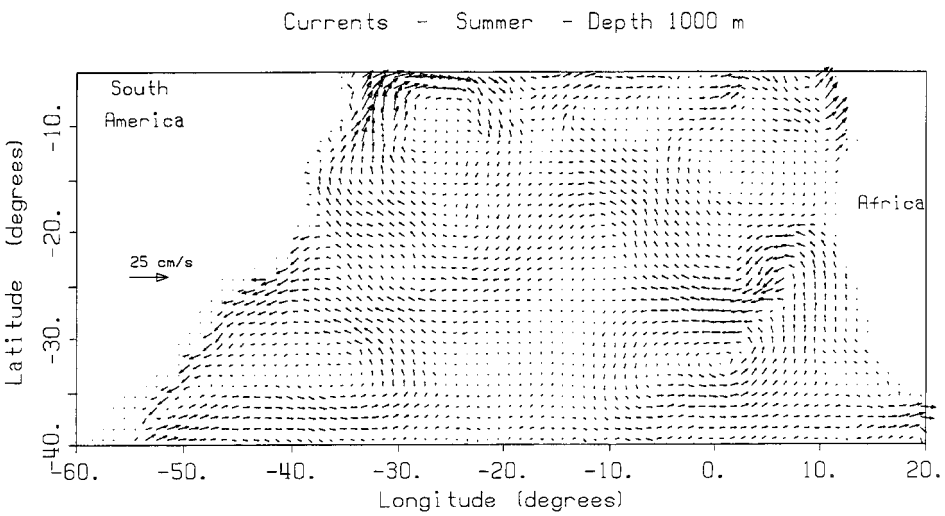

Figure 3. Mean summer horizontal currents at 1000 m depth level.

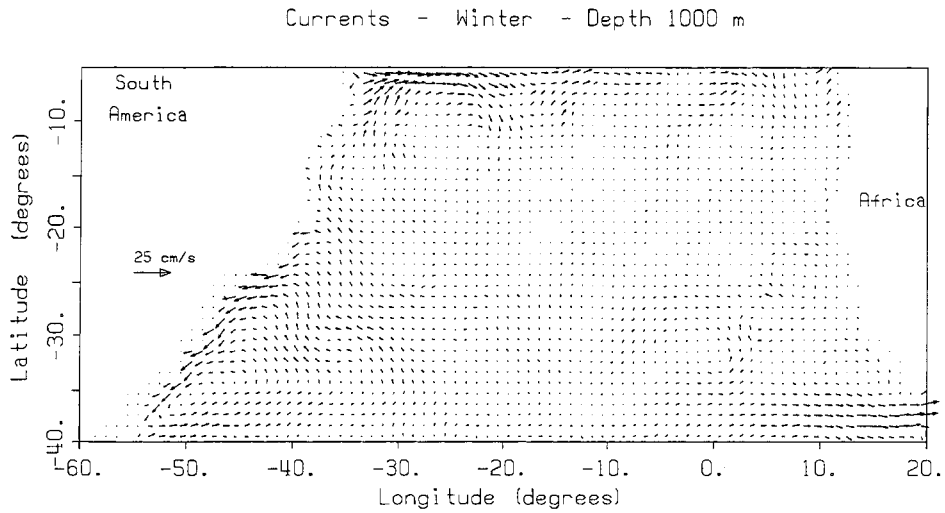

Figure 4. Mean winter horizontal currents at 1000 m depth level.

5. FINAL REMARKS

In this work, the formulation of an ocean circulation model, based on the spectral method for the vertical dependence of the variables, was presented. The basic equations are written in spherical coordinates, in order to allow large-scale simulations, covering the ocean basins.

Although the simplifications made, neglecting the non-linear terms and considering the density field time-invariant, the main features of the South Atlantic gyre were reproduced by

the model, especially the Brazil and Benguela Currents, off the coasts of South America and Africa.

Finally, the adopted formulation is an effective alternative on general circulation ocean models, and the modelists are encouraged to include the non-linear terms and the equations of temperature, salinity and density, in order to perform more realistic simulations.

REFERENCES

1. Bryan K. A numerical method for the study of the circulation of the world ocean. *Journal of Computational Physics* 1969; **4**:347–376.
2. Cox MD. A primitive equation three-dimensional model of the ocean. *GFDL Ocean Group Technical Report No. 1*, GFDL/NOAA, Princeton University, Princeton, 1984; 250 pp.
3. Blumberg AF, Mellor GL. A description of a three-dimensional coastal ocean circulation model. In *Three-Dimensional Coastal Ocean Models*, vol. 4, Heaps N (ed.). American Geophysical Union: Washington, DC, 1987; 208 pp.
4. Bleck R, Rooth C, Hu D, Smith L. Salinity-driven thermocline transients in a wind- and thermohaline-forced isopycnic coordinate model of the North Atlantic. *Journal of Physical Oceanography* 1992; **22**:1486–1505.
5. Davies AM. Formulation of a linear three-dimensional hydrodynamic sea model using a Galerkin-Eigenfunction method. *International Journal for Numerical Methods in Fluids* 1983; **3**:33–60.
6. Davies AM. On computing the three-dimensional flow in a stratified sea using the Galerkin method. *Applied Mathematical Modelling* 1982; **6**:347–362.
7. Davies AM, Stephens CV. Comparison of the finite difference and Galerkin methods as applied to the solution of the hydrodynamic equations. *Applied Mathematical Modelling* 1983; **7**:226–240.
8. Davies AM. Application of a Galerkin-Eigenfunction method to computing currents in homogeneous and stratified seas. In *Numerical Methods for Fluid Dynamics*, Morton KW, Baines MJ (eds). Academic Press: New York, 1982.
9. Hellerman S. An updated estimate of the wind stress on the world ocean. *Monthly Weather Review* 1967; **95**:607–626.
10. Gorshkov SG. *World Ocean Atlas—vol. 2*: *Atlantic and Indian Oceans*. Pergamon Press: Oxford, 1978.
11. Van Loon H. *Climates of the Oceans*, *World Survey of Climatology*. Elsevier Science Publishing Company Inc.: Amsterdam, 1984.
12. Dephant A. *Physical Oceanography*, *vols 1 and 2*. Pergamon Press: Oxford, 1961.
13. Carton JA. Estimates of sea level in the Tropical Atlantic Ocean using GEOSAT altimetry. *Journal of Geophysical Research* 1989; **94**:8029–8039.
14. Meehl GA. *Observed world ocean seasonal surface currents on a 5° grid*. National Center of Atmospheric Research, Boulder, CO, USA, NCAR Technical Note, NCAR/TN/IA - 159 + STR, 1980.
15. Garzoli S, Bianchi A. Time–space variability of the local dynamics of the Malvinas–Brazil Confluence as revealed by inverted echo sounders. *Journal of Geophysical Research* 1987; **92**:1914–1922.
16. Garzoli S, Garrafo Z. Transports, frontal motions and eddies in the Brazil–Malvinas Confluence as revealed by inverted echo sounders. *Deep Sea Research* 1989; **36**:681–703.

